Environmental Energy and Economic Research 2023 7(1): S051
DOI 10.22097/EEER.2022.356717.1263

Research Article

Evaluation of Landscape Dynamics in City Thermal Islands (Case Study: City of Birjand, Iran)

Fatemeh Kafi, Elham Yousefi [*], Fatemeh Jahanishakib

Department of Environmental Engineering, Faculty of Natural Resources and Environment, University of Birjand, Birjand, Iran

Received: 27 July 2022 /Accepted: 15 September 2022

Abstract
One of the most common climatic phenomena associated with urban issues is urban heat islands. Therefore, it is essential for urban planning to study this phenomenon. This article aims to investigate the performance of extraction methods for heat islands and introduce the prior method. Also, identify and analyze the landscape dynamics of heat islands over time in the study area. For this purpose, at first, the land surface temperature (LST) in the city of Birjand, was extracted using the satellite images in the years 2000–2019 in two cold and warm seasons using the mono-window, Planck's equation, radiative transfer equation, and single-channel method in the two seasons of summer and winter. The statistical method of mean absolute error was used for the comparison and selection of the accurate method. The results showed that the accuracy of the single-channel method (Landsat) was higher than other algorithms (MAE = 3.38 °C). The landscape dynamics were also identified using a package of landscape metrics, including PSSD, MPS, CA, NP, and MPFD. On the other hand, during the study period, the summer trend of the city's air quality showed an improvement in the condition of the land in the southern and eastern parts, and the winter trend showed an improvement in the condition of the land in the eastern to northern parts of the city. As a result, the phenomenon of urban heat islands in hot, dry weather causes a decrease in the temperature of the earth's surface with the increase of urban areas.
Keywords: Earth surface temperature, Landsat, Single channel algorithm, landscape metric.

Introduction

The urban heat island (UHI) phenomenon results from an imbalance in surface energy caused by the dramatic changes in the urban landscape. As one of the most evident features of human impact on the Earth system, UHI has been widely documented in almost all major cities worldwide (Wu and Ren, 2018). This transformation, accompanied by the rapid conversion of natural landscapes to impervious surfaces, has resulted in many ecological and environmental problems (Ulpiani, 2021). The air temperature close to the land surface may increase under the influence of UHIs. High urban temperatures exert effects, such as increased energy consumption in buildings, increased concentrations of pollution, reduced environmental sustainability, and reduced human health (Santamouris and Kolokotsa, 2016). As a result of increasing urbanization rates and a decreasing amount of open and green surfaces worldwide,

[*] Corresponding author E-mail: e_yusefi_31@birjand.ac.ir

increasing temperatures and air pollution are found in areas of high energy consumption, causing human health and overall comfort to be adversely affected. The vegetation in cities is affected by this increasing temperature. Further, such temperatures not only change the climate in small areas, but they can also alter a region's climate as a whole. High temperatures lead to considerable decreases in the quantity and quality of water in cities. Because of the increasing temperature and global warming, droughts are becoming an increasingly common occurrence (Soydan, 2020).

Various studies have proved that the rise in temperature raises mortality (Fouillet et al., 2006; Harlan and Ruddell, 2011). Therefore, the research on urban climatology and ecology has mainly focused on ways to reduce and adapt to UHI (Chen et al., 2017; Zhou et al., 2011). A wide range of studies have sought to identify surface UHIs or related LST using the landscape metrics (Table 1). It is believed that the landscape metrics, as a description of landscape patterns, are associated with the weather (Stone and Rodgers, 2001). The use of the ecological landscape approach in land use planning, along with landscape metrics, in the quantitative evaluation of vegetation changes in intact urban areas has attracted more and more researchers. Accordingly, over the two recent decades, studies on the landscape have grown worldwide (Jafari et al., 2015).

The city of Birjand is located in an area with a hot and arid climate and enjoys relatively low vegetation. The city is surrounded by tall mountains. The people migration and high population density over recent decades have created countless building surfaces, such as roofs and walls, as well as pavement surfaces, which usually have dark colors and can absorb considerable solar energy. Heat islands, used in urban climatology, are among the largest threats to the development of urbanization. Therefore, it seems essential to investigate the trend of changes in the heat islands of Birjand from 2000 to 2019. This urban phenomenon is intensified by the alteration of the atmosphere and growth in urbanization (Song and Wu, 2016; Mohammadi and Afifi, 2021).

Previous studies on urban heat islands using satellite images have revealed that in a metropolitan region with a more temperate climate, the areas around the city have always lower temperatures compared to the urban areas. On the other hand, in regions with hot and arid climates, urban areas show lower surface temperatures than their surrounding areas, a phenomenon called urban cold surface islands or urban heat cavities (Lazzarini et al., 2013). This phenomenon is an important consequence of urbanization and urban planning. Using remote sensing science and analyzing the satellite images, this study has investigated the temporal-spatial changes of the heat island of Birjand city to utilize its results in urban planning management of areas. Moreover, based on landscape analysis, it has studied how to change the phenomenon of heat islands according to the LST composition and distribution.

The landscape ecology concepts have been used in numerous subjects, such as evaluation of environmental effects, landscape design, and ecosystem management (Forman and Godron, 1986). Oke (1982) employed these concepts to study UHIs and showed that the landscape composition directly affected the surface temperature. The studies indicate that the land architecture, including the type, size, and pattern of land use and land cover (Turner, 2010) may significantly impact the UHI surface, especially on micro (100 m^2) to local (1 km^2) scales. The relative effects of land cover on LST vary with different uses. Therefore, the importance of land cover to reduce the UHI effects has changed. For instance, in industrial/commercial zones mainly covered with buildings and impervious surfaces, the presence of buildings is associated with high temperatures. On the other hand, buildings have a reverse relationship with temperature in residential areas. Given its effect on radiative and energy flows, the spatial distribution of landscape plays an important role in determining the surface temperature and formation of UHIs (Connors et al., 2013).

Table 1. The background of studies on the identification of UHI and applications of landscape metrics

Writers	Year	Subject of study	LST extraction method	Calculated metrics
Xiang et al.	2022	Seasonal variations for combined effects of landscape metrics on land surface temperature (LST) and aerosol optical depth (AOD).	brightness temperature	PLANDT, LPI, AI, SHAPE_MN
Effati et al.	2021	Investigating effects of land use and land cover patterns on land surface temperature using landscape metrics in the city of Tehran, Iran.	standard deviation and quartile deviation methods	PLAND, MPS, AI, PAFRAC, COHESION, CONTAG, SHDI
Feng et al.	2021	Urban ecological land and natural-anthropogenic environment interactively drive surface urban heat island: An urban agglomeration-level study in China.	impervious surface distribution density (ISDD) method, and city clustering algorithm (CCA)	PEL, PD, SHAPE, LPI, AI, SHDI
Pramanik and Punia	2020	Land use/land cover change and surface urban heat island intensity: source–sink landscape-based study in Delhi, India.	single-channel algorithm	LI
Soydan	2020	Effects of landscape composition and patterns on land surface temperature: Urban heat island case study for Nigde, Turke.	supervised classification method	LUCC
Yao et al.	2020	How the landscape features of urban green space impact seasonal land surface temperatures at a city-block-scale: An urban heat island study in Beijing, China.	Radiative Transfer Equation algorithm	Total area, Patch density, Landscape shape index, Shannon's diversity index, Per cent of landscape, Largest patch index, Edge density, Aggregation index
Pan et al.	2019	Characterizing urban redevelopment process by quantifying thermal dynamic and landscape analysis.	Planck's equation	PD, AI, PAFRAC, LSI SHDI, MSIDI
Yu et al.	2019	Strong contribution of rapid urbanization and urban agglomeration development to regional thermal environment dynamics and evolution.	Radiative Transfer Equation algorithm	LUTM
Tang et al.	2018	Effect analysis of land-use pattern with landscape metrics on an urban heat island.	Radiative transfer equation algorithm	PLAND, ED, AREA_MN, ENN_MN, SHEI
Estoque et al.	2017	Effect of landscape composition and pattern on land surface temperature: An urban heat island study in the megacities of Southeast Asia.	L8SR algorithm	MPS, MSI, AI
Zhou et al.	2017	Effects of the spatial configuration of trees on urban heat mitigation: A comparative study.	Planck's equation	AREA_MN, ED, SHAPE_MN, LPI

Table 1. (continued). The background of studies on the identification of UHI and applications of landscape metrics

Writers	Year	Subject of study	LST extraction method	Calculated metrics
Li et al.	2017	Linking potential heat source and sink to urban heat island: Heterogeneous effects of landscape pattern on land surface temperature.	Semi-parametric geographically weighted regression (SGWR) model	LAND (PD, CONTAG, SHDI, AI) CLASS (PLAND, NP, PD, LPI, ED, LSI, SHAPE_MN, SHAPE_AM, FRAC_MN, FRAC_AM, DIVISION, AI
Gage et al.	2017	Relationships between landscape pattern metrics, vertical structure and surface urban Heat Island formation in a Colorado suburb.	Random regression models (RRM)	CLASS (AREA_MN, CLUMPY, COHESION, ED, GYRATE_MN, IJI, LPI, LSI, NLSI, NP, PD, PLAND) LAND (AI, CONTAG, IJI, LPI, LSI, NP, PD, PR, PRD, SHDI, SIDI, DIVISION, SIEI)
Song et al.	2014	The relationships between landscape compositions and land surface temperature: Quantifying their resolution sensitivity with spatial regression models.	Spatial regression model	Land Scape Shape Index, and Edge and Patch Density
Chen et al.	2014	How many metrics are required to identify the effects of the landscape pattern on land surface temperature?	Cluster analysis, factor analysis, and regression	COHESION, MESH, SPLIT, LPI, PLAND, PROX MN, AI, CORE MN, DCAD, ENN MN, ED, LSI, DCORE MN, PROX AM, PD, CONNECT, DIVISION, CLUMPY, NLSI, FRAC MN, SHAPE MN, CONTIG MN

Various metrics have been developed to evaluate these effects (Song et al., 2014). Over recent decades, landscape science has provided the hypotheses and tools required for the evaluation of the properties of the urban ecological structure. A wide range of research has sought to identify surface UHI or related LST using landscape metrics (Connors et al., 2013; Liu et al., 2011). It is believed that the landscape metrics, as a description of landscape patterns, are related to climate (Stone and Rodgers, 2001). Various metrics have been suggested to measure the landscape patterns, including the composition and characteristics of the land use/land cover configuration (Uuemaa et al., 2013; Kupfer, 2012). A review of previous studies reveals that the modeling of the relationship between landscape metrics, land use, and heat islands has attracted considerable attention from researchers.

However, an innovation of this research in the second section is that the research has focused on the landscape dynamics of heat islands in different periods. Therefore, an analysis of the series of spatial changes, the intensity of heat islands, and the coaction between the factors effective in heat islands in the city was obtained, which indicated the trend and degrees of environmental quality and climatic comfort in different areas of Birjand city. Furthermore, the majority of studies were carried out in humid suburbs with dense vegetation, but this study was conducted in a dry, desert region with little to no vegetation, which produced different results. On the other hand, the present study is a combination of multiple cases (including changes in

various times, seasons, different algorithms, and analysis of various metrics of the landscape) that have all been studied individually in other studies.
The goals of the present study include:

1. Identification of heat islands and critical points of Birjand city.
2. Evaluation of changes in heat islands over the past 19 years in the city with an acceptable resolution
3. Analysis of landscape dynamics of heat islands to determine the favorability degrees of climatic comfort in different areas of Birjand city.

Material and Methods

Identification of the study area

Figure 1 demonstrates the location of the study area in Birjand city, with an area of 4004 km^2. Birjand has a height of 1491 m above mean sea level. The city is the capital of the Southern Khorasan Province, which is located in eastern Iran, on the northeastern side of the Lut Desert. Birjand is located between the latitudes of 31°20'N and 33°31'N and longitudes of 57°57'E and 59°40'E.

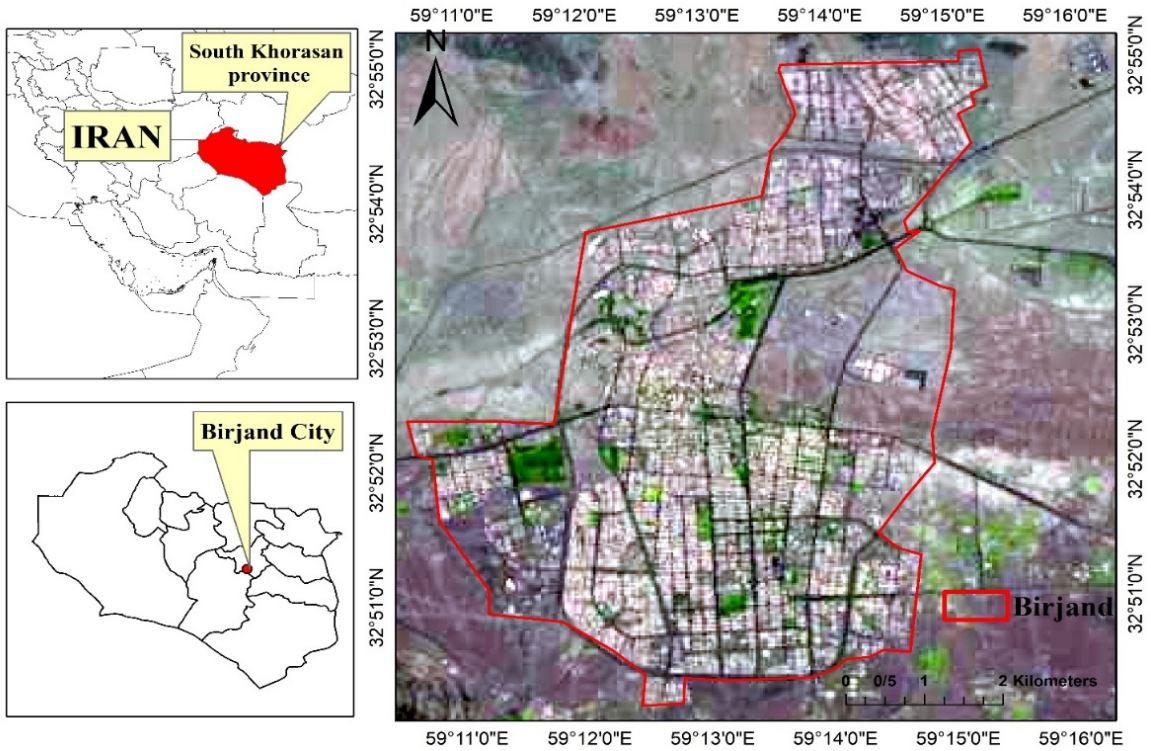

Figure 1. The location of the study area in the Southern Khorasan Province, Iran

Research data

Four different satellite images related to summers and winters from 2000 to 2019 were used to investigate the phenomenon of urban heat in Birjand. The images of the Landsat 7 and 8 sensors were obtained from the United States Geological Survey (USGS) website, whose details are provided in Table 2. The image of the public zone of Birjand was located in zone 40 in the UTM imaging system with a row number of 37 and a path number of 159.

The temperature data of the Birjand weather station were also obtained from the https://www.ogimet.com/gsynres.phtml.en website (Table 3).

Table 2. Satellite images used in the research

Row	Satellite type	Sensor type	Survey date (Gregorian)	Survey date (Solar Hijri)	Survey time (GMT)	Survey time (Tehran)
1	Landsat8	TIRS/OLI	2019/01/01	1397/10/11	06:37:52	11:07:52
2	Landsat8	OLI/TIRS	2019/07/12	1398/04/21	06:37:56	11:07:56
3	Landsat7	ETM+	2000/01/21	1378/11/01	06:30:47	11:00
4	Landsat7	ETM+	2000/07/15	1379/04/25	06:29:28	10:59:28

Table 3. The temperature properties of Birjand weather station

Data	Temperature (°C)			Average relative humidity (%)	Wind speed (Km/h)	Pressure (Hp)	Sunshine hours (h)
	Maximum temperature	Minimum temperature	Mean temperature				
2019/1/1	13.3	-1.9	4.5	47.6	15.3	854.6	8.4
2019/7/12	38.3	21.5	30.8	15	19.8	842.2	12.4
2000/1/21	13.4	5.6	8.5	67.7	6.2	846.2	8.4
2000/7/15	33	15.6	26.3	26.7	6.4	845.1	*

LST estimation procedure

Conversion of DN to radiance

The conversion of digital values of images to radiative values using the conversion function, Equation 1, is among the most important points of analysis in this study (Chander et al., 2009).

$$L\lambda = \frac{(LMAX\lambda - LMIN\lambda)}{(Qcal\ max - Qcal\ min)} * (Qca - Qcal\ min) + LMIN\lambda \quad (1)$$

$L\lambda$: indicates the spectral radiance value.
Qcal: Denotes the digitalized value of calibrated *DN*.
Qcal min: Is the minimum value of *Qcal* corresponding with $\lambda LMIN$.
Qcal max: Is the maximum value of *Qcal* corresponding with $\lambda LMAX$.
LMIN and *LMAX*: Indicate the minimum and maximum radiative radiances whose values are 0 and 255 $wm^{-2}sr^{-1}\mu m^{-1}$, respectively. In atmospheric corrections of the atmospheric environment on the main image, it is often assumed to be similar (Aliabadi and Soltanifard, 2017).

Conversion of radiance to lighting temperature

Lighting temperature is the temperature corresponding with the radiative energy reflected from the surface of a phenomenon by a sensor, which is obtained by Equation 2 (Beigi et al., 2013).

$$TR = \frac{K2}{Log\ (\frac{K1}{L\lambda} + 1)} \quad (2)$$

TR: Lighting temperature (K)
$L\lambda$: Spectral radiance ($wm^{-2}sr^{-1}\mu m^{-1}$)
K_1 and K_2: Calibration coefficients of sensor ($wm^{-2}sr^{-1}\mu m^{-1}$)

Calculation of normalized difference vegetation index (NDVI)

NDVI is widely used in urban studies. According to studies, NDVI significantly absorbs the red band, while intensely reflecting the infrared band (Moghimi et al., 2017).
NVDI is among the commonest indexes proposed to evaluate the vegetation status, which is calculated by Equation 3 (Atzberger, 2013).

$$NDVI = \frac{Bnir - Bred}{Bnir + Bred} \quad (3)$$

Bnir: Level of reflection in the infrared band
Bred: Level of reflection in the red band

Calculation of surface emissivity

Surface emissivity is among the most effective parameters for estimating LST. It equals the ratio of thermal energy reflected by a surface to the thermal energy reflected from a black body at the same temperature.

For LAI<3
$$\varepsilon NB = 0.97 + 0.0033 * LAI \quad (4)$$
For LAI ≥ 3
$$\varepsilon NB = 0.98$$

NB equals 0.99 for water and snow (Beigi et al., 2013).

Second method: Given the mix of each pixel in some studies, surface emissivity in each pixel is calculated through Equation 5 (Sobrino et al., 2004).

$$\varepsilon = \varepsilon v Pv + \varepsilon s(1 - Pv) + d\varepsilon \quad (5)$$

In Equation 5, $\boldsymbol{\varepsilon}_v$ denotes the vegetation emissivity, $\boldsymbol{\varepsilon}_s$ is the soil emissivity, and p_v represents the vegetation ratio. Parameter $d\boldsymbol{\varepsilon}$ is calculated through Equation 6.

$$d\varepsilon = (1 - \varepsilon s)(1 - Pv)F\varepsilon v \quad (6)$$

In which *F* is the shape factor, being equal to 55% (Sobrino et al., 1990).
According to studies, the emissivity of vegetation, soil, and urban structure is equal to 99%, 97%, and 92%, respectively. Accordingly, emissivity is calculated through Equation 7 (Liu et al., 2011).

$$\varepsilon = 0.02644PV + 0.96356 \quad (7)$$

LST calculation algorithms

A goal of this study is to determine the most accurate method for LST calculation in Birjand city. For this purpose, the four methods of the single-channel algorithm, radiative transfer equation, mono-window algorithm, and Planck's equation were used. The most accurate method was chosen by comparing their results with the land data. Afterward, the analysis of landscape metrics was performed on the final map resulting from the chosen method.

Planck's equation

A brightness temperature image and an emissivity image are required in order to estimate LST. Due to the lack of atmospheric correction, Planck's equation is limited compared to other methods. This algorithm includes the following stages:

1. Calculation of thermal radiance in ENVI software

2. Calculation of brightness temperature in QGIS software
3. Calculation of NDVI in QGIS software

A) Calculation of atmospheric radiometric corrections for blue to near-infrared bands in ENVI software

B) Getting the output from red and near-infrared bands in TIFF format

4. Calculation of emissivity in QGIS software

Emissivity is essential to converting brightness temperature to kinetic temperature. The brightness temperature is the temperature of the black body at a given wavelength (11.5 μm) (Shakiba et al., 2009). LST is finally calculated using Planck's equation.

Mono-window algorithm

The mono-window algorithm has been suggested by Qin et al. (2001) to retrieve the LST mono-window algorithm. It necessitates three major parameters: diffusion, transmission, and average atmospheric temperature. Band 6 of Landsat ETM+ and band 10 of Landsat 8 record radiation with a spectrum of 10.4 mm to 12.50 mm for Landsat ETM+ and 10.60 mm to 11.19 mm for Landsat 8 (Chen et al., 2014). This algorithm is among the new precise methods to calculate the LST. For this purpose, the parameters like brightness temperature, average atmosphere temperature, atmospheric transmission coefficient, and emissivity are used to calculate LST. By using this algorithm, it is possible to calculate the LST in a corrected way. The mono-window algorithm is more accurate compared to other methods and can be used for Landsat and Aster data. The atmospheric transmission coefficient is calculated using the NASA website, and Equation 8 gives the average atmosphere temperature (in Kelvin).

$$Ts = \frac{\{a(1-C-D)+[b(1-C-D)+C+D]Ti - D*Ta\}}{C} \quad (8)$$

$$C = \varepsilon i * \tau$$

$$D = (1-\tau)(1+(1-\varepsilon i)*\tau)$$

a= -67.355351 and b= 0.4558606

εi: Land surface emissivity

Ti: brightness temperature on the sensor's surface

τ: Atmospheric transmittance

Ta: Average effective air temperature

Ts: Land surface temperature (Kelvin)

t: Temperature (°C)

$$Average\ atmospheric\ temperature\ = 16.011 + (0.92621 * (t + 273.15)) \quad (9)$$

Algorithm of the radiative transfer equation

This algorithm is used for Landsat data, and TM, ETM+, and OLI/TIRS sensors. To calculate LST, it uses the parameters, such as atmospheric upward and downward radiations, atmospheric transmission coefficient, and emissivity, and creates a proper atmospheric correction. The upward and downward radiations and the atmospheric transmission coefficient are calculated using the NASA website.

Single-channel algorithm

The single-channel algorithm is among the most important algorithms widely used to calculate LST in remote sensing. It calculates LST in the form of atmospheric correction, which improves

its accuracy. The algorithm uses the radiance images, brightness temperature, and emissivity, along with the atmospheric correction parameters of thermal bands. Equation 10 is the general form of the algorithm.

$$Ts = \gamma(1\varepsilon(\varphi 1\ lsen + \varphi 2) + \ \varphi 3) + \delta \tag{10}$$

$$\gamma \approx \frac{Tsen2}{b\gamma lsen} \tag{11}$$

$$\delta \approx Tsen - \frac{Tsen2}{b\gamma} \tag{12}$$

$$\varphi 1 = \frac{1}{\tau} \tag{13}$$

$$\varphi 2 = -Ld - \frac{Lu}{\tau} \tag{14}$$

$$\varphi 3 = Ld \tag{15}$$

T_S: Land surface temperature (Kelvin)
$\boldsymbol{\varepsilon}$: land surface emissivity power
$lsen$: Radiance on the sensor's surface
$Tsen$: Brightness temperature on the sensor's surface
τ: Atmospheric transmissibility
Ld: Downward atmospheric radiation, and
Lu: upward atmospheric radiation, which indicates the availability of atmospheric radiosonde data close to the study area and close to receiving the satellite images (Yang and Liu, 2005).

The single-channel algorithm employs the parameters of water vapor existing in the atmosphere, and since the water vapor absorbs thermal infrared waves, the effect of the molecules can be estimated based on the electromagnetic waves. Equation 16 gives the atmosphere water vapor.

$$Wi = 0.0981 * \left\{10 * 0.6108 * exp\left[\frac{17.27 * (T0 - 273.15)}{273.3 + (T0 - 273.15)}\right] * RH\right\} + 0.1679 \tag{16}$$

Wi: Atmosphere's water vapor
$T0$: Temperature of a station on the land surface (°C)
RH: Relative humidity (%)

Landscape dynamics of heat islands

The map obtained from the prior algorithm (single-channel) was used to identify the landscape dynamics of heat islands in Birjand. The analysis of spatial changes and intensity of thermal islands was performed in the landscape hexagonal network due to the proper cover of the study boundaries and having more proximity. Each hexagon in this network is a single analysis known by sub-landscape blocks.

In this study, different compositional and distributional landscape metrics were used at the class and landscape levels. The landscape metrics of PSSD, MPS, NP, CA, and MPFD were calculated using the Patch Analyst software package in the class and landscape levels inside the hexagonal units (Table 4 summarizes the metrics used in the study). Accordingly, in order to identify the landscape changes, the desired metrics were calculated for two periods in the years 2000 and 2019 in the summer and winter seasons.

Table 4. Landscape metrics

Metric	Abbreviations	Definitions	Equation	Unit
Metric type: Composition				
Class area	CA	It calculates the total area of one type of patches.	A	h
Metric type: Distribution				
Number of patches	NP	It is the total number of patches in the landscape	NP =N	-
The average size of the patch	MPS	It is the average size of the patch.	$\frac{\sum_{i=1}^{n} a_{ij}}{n_i}$	h
Patch size standard deviation	PSSD	The standard deviation of the patch from all patches in a specific classification	$\sqrt{\frac{(\sum_{j=1}^{n}(a_{ij}-(\sum_{i=1}^{n} a_{ij}))^2}{n_i}\left(\frac{1}{1000}\right)}$	h
Mean patch fractal dimensions	MPFD	It is the mean dimensions of the patch compaction. As it is closer to unity, the patch is more uniform.	$\frac{\sum_{j=1}^{n} \frac{2\ln p_{ij}}{ln a_{ij}}}{n_i}$	-

The landscape dynamics analysis was performed based on the effect of metrics and intensity degrees of heat islands on the quality of the urban environment. The urban areas were classified into various periods based on different metrics. Accordingly, the intensity classification map of heat islands was analyzed by landscape metrics. The integration of each metric in each period was performed based on the intensity classification map of heat islands separately. Then, Equation 17 was used to aggregate the effect of each class and obtain the rank of each metric in sub-landscape units.

$$(Metricx\_Class1 * 1) + (Metricx\_Class2 * 2) + (Metricx\_Class3 * 3) + (Metricx\_Class4 * 4) + (Metricx\_Class5 * 5 = \text{Rank of sub-landscape block} \quad (17)$$

Eventually, the summer and winter dynamics of heat islands were evaluated by aggregation of the rank of landscape metrics in each period and classifying them based on the effectiveness in the number of urban areas.

Results

The images of temperature classes for the 19-year period from winter 2000 to summer 2019 were extracted by calculating and extracting the images of variance, brightening temperature, emissivity, and NDVI. The LST calculated using the mono-window, Planck's equation, radiative transfer equation, and single-channel algorithms. The LST calculated in these images was in the range of 1°C to 51°C.

The urban land use, worn-out urban fabric, and vegetation had the lowest LST while the use of barren lands had the highest LST. The classification with small samples of large-scale data is important in many areas. Quantile classifications are the distance-based classifications that

require a single parameter regardless of the dimension. They classify the observations with respect to the sum of weight distances inside the classes (Hennig and Viroli, 2015). In a quantitative quantile classification, each class includes a given number of characteristics. The quantitative classification is very suitable for linearly distributed data. Quantile allocates data to each class in the same number of values. There are no empty classes with very low or very high values (Osaragi, 2002). A positive aspect of quantitative classification is that almost the same number of observations in each class is shown on the map, which allows the reader to properly understand the distribution (Mease et al., 2007). In this research, five classes were used for the quantile classification system. The temperature data of the Iran Meteorological Organization were utilized to validate the temperature data extracted from band 6 of ETM+ and band 10 of TIRS/OLI sensors. Since the satellite passes through the study area at 6:30 AM GMT and 11:00 AM local time, the available data of 6:00 AM GMT, one hour before the imaging, was used to compare the LST with the temperature of the soil at a depth of 5 cm in the Birjand synoptic station.

Table 5 demonstrates the difference between the LST calculated from images and the temperature of soil measured at a depth of 5 cm in the synoptic station. There is a direct relationship between the temperature at a depth of 5 cm in the soil and the soil surface temperature. The rise in the soil surface temperature changes the temperature of different depths of the soil with time delays. In other words, the temperature increases or decreases at the soil surface, and then, the rise or decline occurs at various depths of the soil. The mentioned temporal difference is directly related to the soil depth (Alavipanah, 2007). For instance, the average error in the single-channel method is about 3.38°C, and this method is the most precise method with the lowest error to prepare the LST map of Birjand. Figure 2 illustrates the maps obtained using this method.

Table 5. A comparison between the LST calculated from images and the temperature of soil measured at a depth of 5 cm in the synoptic station

Mean absolute error (MAE)	The difference between LST and soil temperature in the station	The temperature at a depth of 5 cm of the soil in the station	The LST calculated from the images	Algorithm type	Station name	imaging date
8.20	6.64	12/4	19/04	Mono-windows	Birjand	2000/1/21
	13.46	39/6	53/06		Birjand	2000/7/15
	8.68	10/4	19/08		Birjand	2019/01/01
	4.04	45/4	49/44		Birjand	2019/7/12
5.18	5.47	12/4	17/87	Planck relation	Birjand	2000/1/21
	7.17	39/6	46/77		Birjand	2000/7/15
	7.56	10/4	17/96		Birjand	2019/01/01
	0.52	45/4	45/92		Birjand	2019/7/12
6.61	6.11	12/4	18/51	Radiation Transfer Equation	Birjand	2000/1/21
	12.64	39/6	52/24		Birjand	2000/7/15
	3.97	10/4	14/37		Birjand	2019/01/01
	3.75	45/4	49/15		Birjand	2019/7/12
3.38	0.34	12/4	12/74	Single channel (Landsat)	Birjand	2000/1/21
	5.96	6/39	45/56		Birjand	2000/7/15
	6.55	10/4	16/95		Birjand	2019/01/01
	0.68	45/4	44/72		Birjand	2019/7/12

It yields results far from the reality since the output of all LST methods is land surface temperature.

$$MAE = \frac{|X_k - Y_k|}{K} \tag{18}$$

K: Number of data

X_K-Y_K: The difference between the remote sensing results and ground data.

The MAE values closer to zero indicate lower error compared to the standard mode (Shahabifar et al., 2010).

According to Figure 2(c), it can be found that the temperature class area of 47-51°C in summer 2000 was the smallest, while the temperature class of 45-46°C had the largest area in the same year. Meanwhile, the area of temperature classes in Figure 2(a), 2(b) and (d) have shown an almost constant trend. So, Figure 3 demonstrate the classified UHI maps used in relation to the land uses.

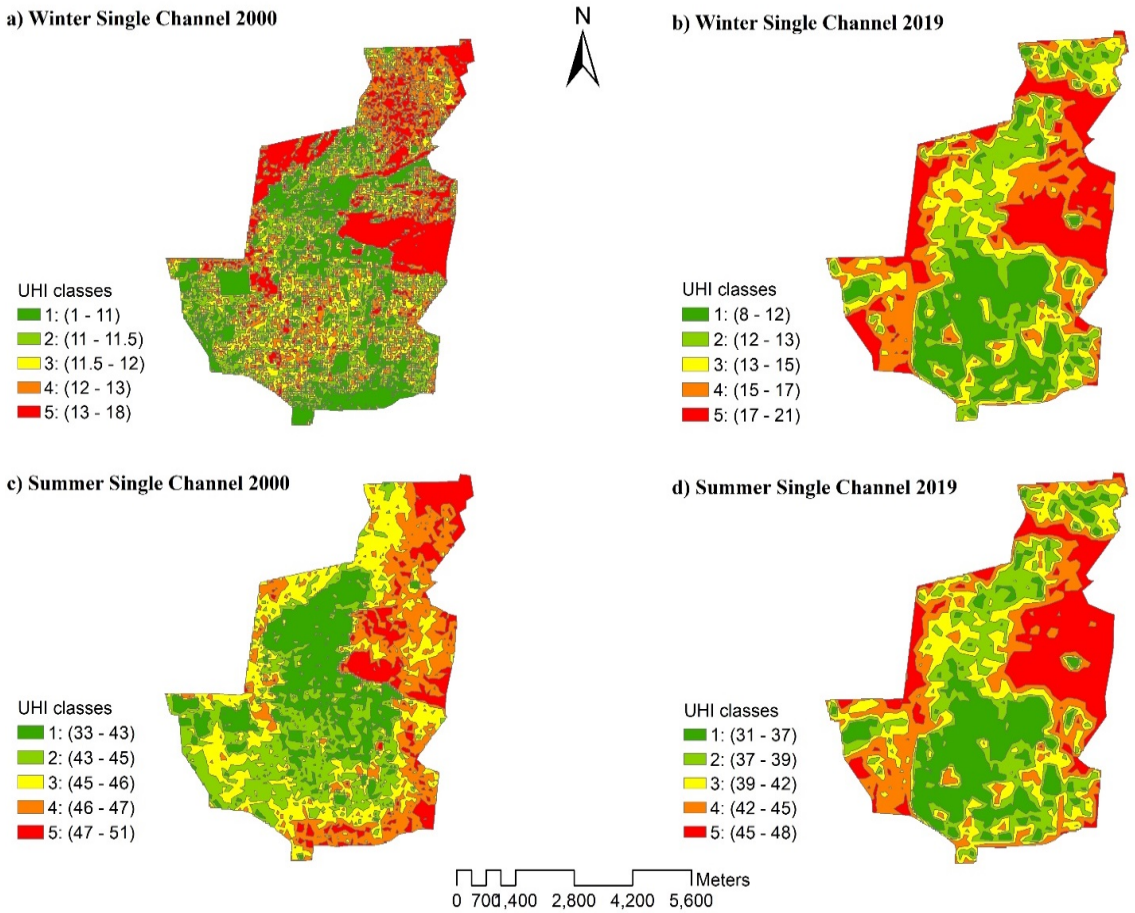

Figure 2. The images of the LST map obtained from the single-channel algorithm

On the whole, According to Figure 3 thermal maps extracted from the LST calculation methods in this study, the green space and residential land uses were in the lowest temperature class, being included in the cold islands of Birjand city. Meanwhile, the temperature of industrial land uses, barren lands, and downtown was in the highest temperature class, being included among the heat islands of Birjand.

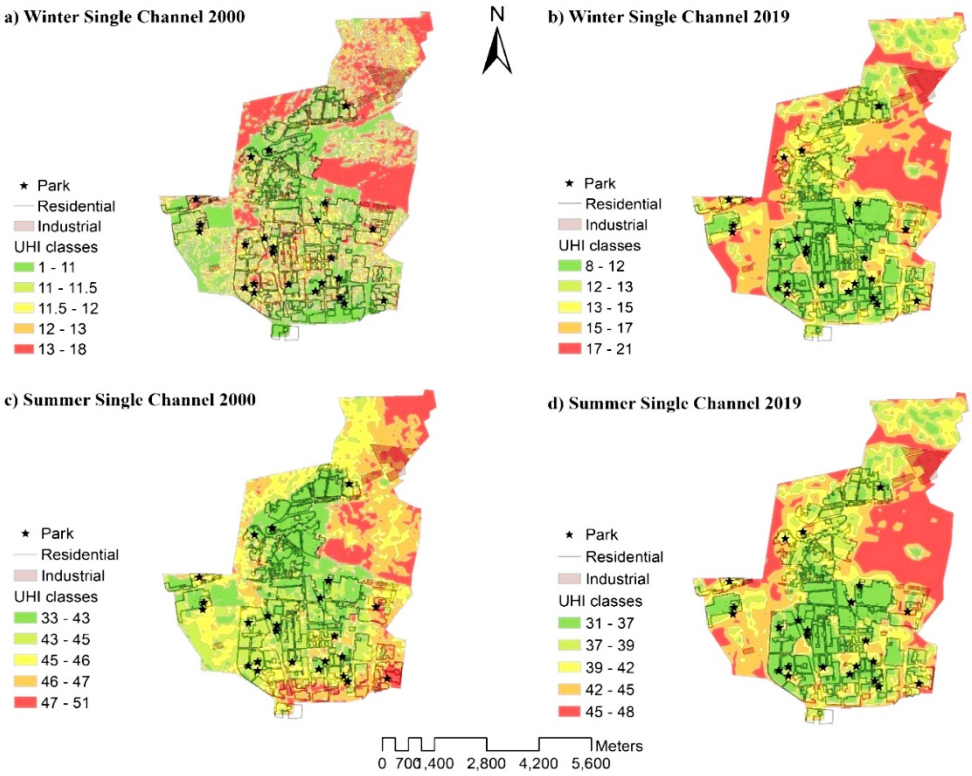

Figure 3. Overlay the land use and heat island maps using the single-channel algorithm

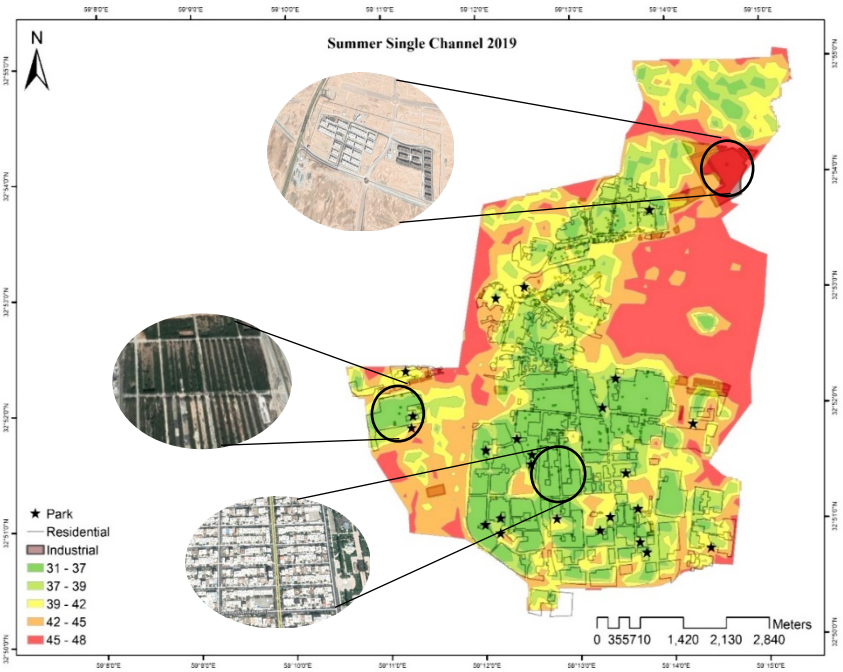

Figure 4. Examples of location of heat and cold islands of Birjand in the single-channel algorithm, summer 2019

The map showing the location of residential, commercial, and green space areas in summer 2019 (Figure 5). According to the curves, the temperature has decreased in residential areas and green space while increasing in commercial areas.

Figure 6 shows the temperature trend using the single-channel algorithm in summer 2019 for the location of residential, commercial, and green space land use shown.

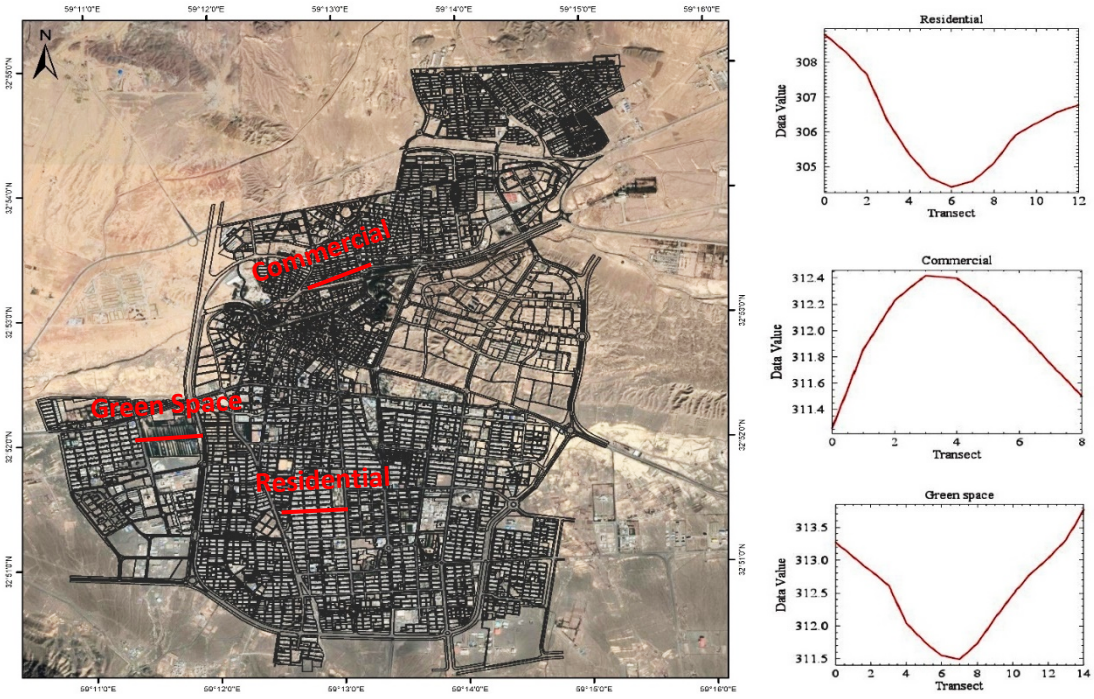

Figure 5. The temperature histogram of the single-channel algorithm in summer 2019

The results of landscape dynamics of heat islands

The landscape evaluation of the heat islands in summer indicated the higher quality of landscape status in the blocks of the west, south, and some central parts of Birjand in 2000. Equation 6(a) illustrates the landscape quality level of summer in Birjand in 2000. Equation 6(b) indicates the landscape quality levels based on the resultant calculated metrics in summer 2019. In this figure, the blocks west of the city have still low quality, while the blocks south of the city have better conditions. Each metric expresses the condition of a heat island landscape that exerts a different effect on the landscape quality and favorability. Although the metrics were integrated using the method mentioned in the. Equation 16, the changes in each metric and the way they yielded effects were considered as follows.

The more the class area (CA), there is larger total area. Therefore, the quality of ecological conditions declines, and the heat island is intensified, resulting in the lower urban environmental quality in such conditions. Figure 1s in the appendix depicts the summer and winter trend of CA metrics in various periods.

The number of patches (NP) indicates the level of spatial heterogeneity and fragmentation of heat island patches, which affect ecological processes. The rise in NP leads to instability and lower quality in the environment. Figure 2s in the appendix depicts the summer and winter trends of NP metric in various periods.

The lower MPS of heat island patches in the studied blocks indicates the fragmentation conditions in the landscape, which lowers the urban environment. Figure 3s in the appendix illustrates the summer and winter trends of MPS metric in various periods.

The PSSD values closer to zero indicate the equal sizes of all heat island patches and improved conditions of the urban environment. Figure 4s in the appendix demonstrates the summer and winter trends of PSSD metric in various periods.

MPFD indicates the mean patch fractal dimensions. The rise in this metric increases the disorder in an image. It is the average compactness dimensions of a patch. As it is closer to unity, the patch is more uniform, resulting in stability in the environment and reducing heat

islands. Figure 5s in the appendix shows the summer and winter trends of the MPFD metric in various periods.

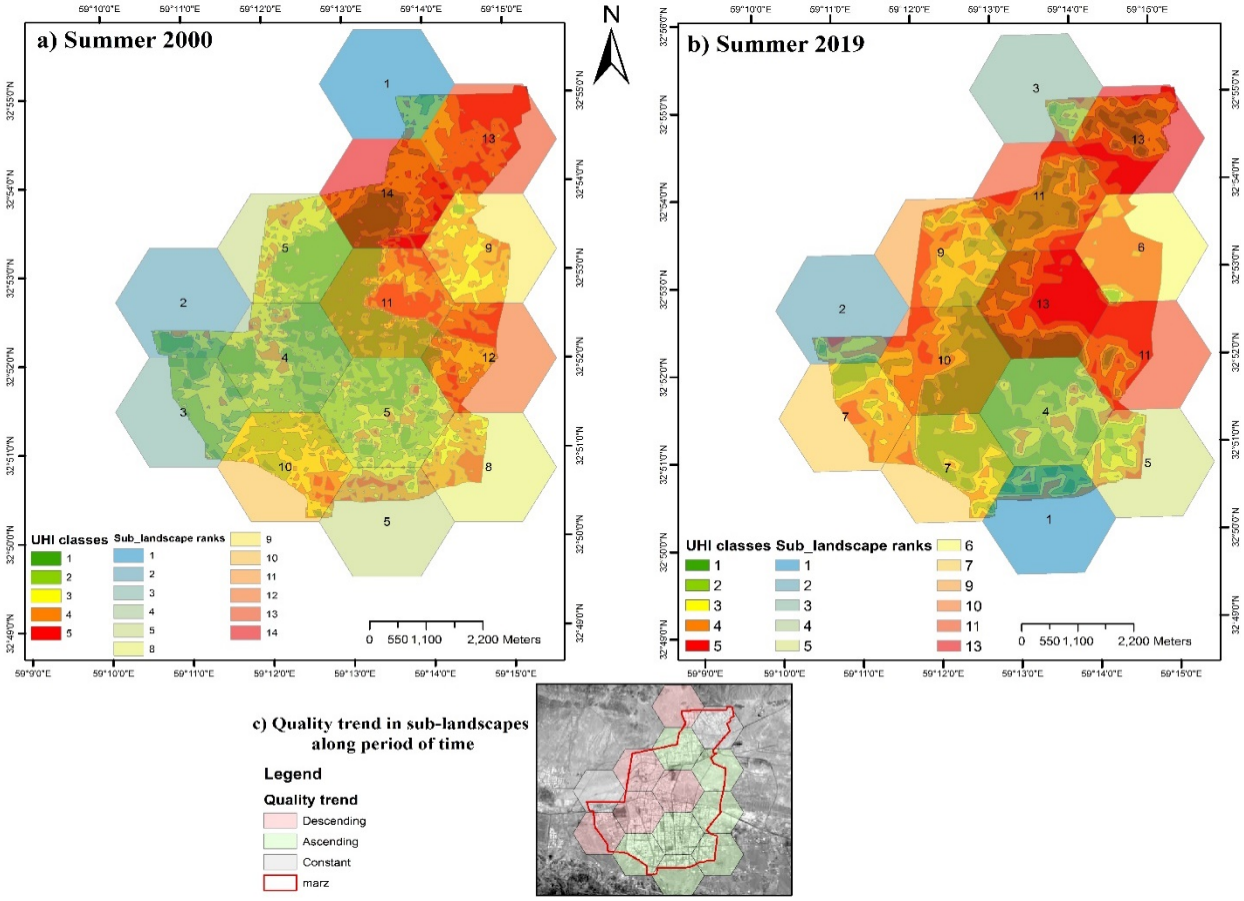

Figure 6. Status of heat island landscapes and summer trend in the years 2000 and 2019

The summer trend of urban air quality in the studied blocks in 2000 and 2019, as shown in Figure 6(c), indicates the improved condition of landscape in the southern and eastern parts of the city. Although the quality level of western blocks is better than the eastern ones according to their ranks, no improvement trend is observed in the western blocks of the city. As a general fact observed in summer, the southern and western areas of Birjand have a favorable air corridor, which is a path enjoying better quality.

The landscape dynamics evaluation of the heat islands in winter indicated the higher quality of landscape status in the western and southern blocks of Birjand in 2000. Equation 7(a) illustrates the landscape quality level of winter in Birjand in 2000. Figure 7(b) indicates the landscape quality levels based on the resultant calculated metrics in winter 2019. In this figure, the central and northwestern blocks of the city have still low quality, while the southern and eastern blocks of the city have better conditions. The winter trend of urban air quality in the studied blocks from 2000 to 2019, as shown in Equation 7(c), indicates the enhanced status of landscape in the eastern to northern parts of the city. As a general fact perceived from the landscape analysis of winter 2019, there is a desirable winter air quality corridor from the south to the east and northeast of Birjand, which is a path with higher quality in terms of the composition and distribution of heat islands.

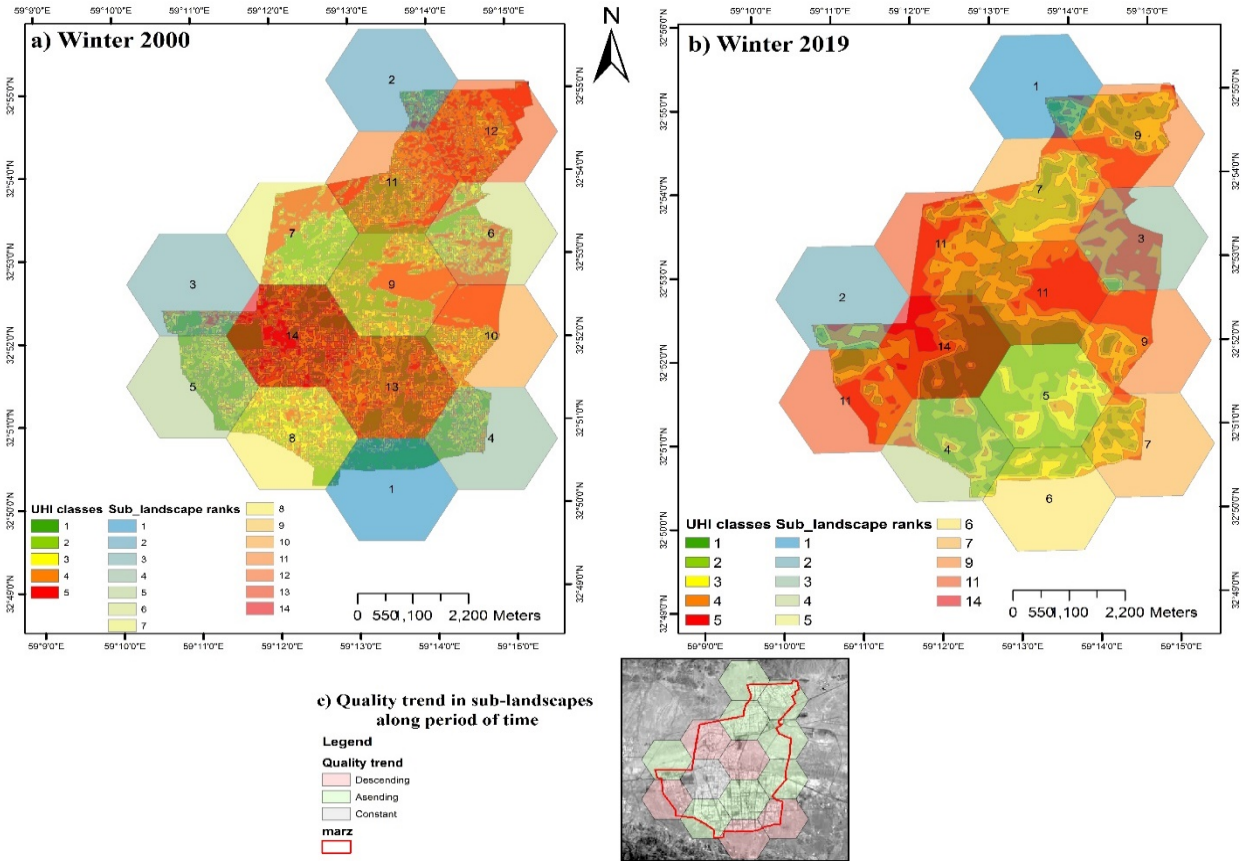

Figure 7. Status of heat island landscapes and summer trend in the years 2000 and 2019

Discussion

One of the key parameters in the analysis of cities is the temperature of the earth's surface. Studying its relationship with the ecological structure of cities gives us a correct understanding of its impact on urban heat islands in order to improve and sustain the environment. In this research, mono-window, Planck's equation, radiative transfer equation, and single-channel method algorithms were used to investigate the temperature of the earth's surface.
Because of its greater accuracy, the single-channel method (Landsat) was chosen over other methods and this method was used to extract LST. Fekrat et al. (2020) measured the earth's surface temperature using four single-channel algorithms (Landsat), improved single window, inverse relation of Planck's function, and radiation transfer equation.

The results showed that the single-channel method (Landsat) is more accurate than other methods. The result of which is consistent with the present study. Afterward, the landscape metrics of MPS, NP, CA, PSSD, and MPFD were calculated using the Patch Analyst software package for the intended sub landscape blocks for images of winter 2000, winter 2019, summer 2000, and summer 2019 of the single-channel algorithm. Since Birjand is located in a hot and arid region, the buildings acted as cold islands. The review of literature on urban heat islands using satellite images has revealed that in a metropolitan region with a more temperate climate, the areas around the city have always lower temperatures compared to the urban areas. On the other hand, in regions with hot and arid climates, urban areas show lower surface temperatures than their surrounding areas, a phenomenon called urban cold surface islands or urban heat cavities (Lazzarini et al, 2013). This was confirmed in this research. According to thermal maps extracted from the LST calculation methods in this study, the green space and residential land uses were in the lowest temperature class, being included in the cold islands of Birjand city.

Meanwhile, the temperature of industrial land uses, barren lands, and downtown was in the highest temperature class, being included among the heat islands of Birjand.

In a study on the effect of heat islands of developed and undeveloped lands on each other using thermal and reflective remote sensing data, Karimi Firozjaei et al. (2019) also found that the LST of green spaces and agricultural lands increases at smaller distances from developed lands. The developed lands directly affect the LST of their surrounding lands, and the undeveloped lands in the higher temperature class are positioned at closer average distances to the developed lands compared to the lower temperature class. This finding was also approved in this study. Also, Connors et al. (2013) showed that the vegetation surfaces and impermeable surfaces in residential areas have more proper temperatures compared to the industrial and commercial uses. Ahmadi et al. (2015) investigated the temperature difference and effective role of vegetation on the pattern of heat islands in cities during the warm days of the year. They emphasized the role of vegetation in reducing the thermal islands, which was also approved for Birjand in the current study. The results of this research also agree with the studies of Ahmadi et al. (2016) on the effect of satellite images and normalized difference vegetation index (NDVI) to identify the pattern of urban heat islands. According to the landscape metrics of MPS, NP, CA, PSSD, and MPFD, the summer trend of urban air quality in the studied blocks in 2000 and 2019, indicates the improved condition of landscape in the southern and eastern parts of the city. The winter trend of urban air quality in the studied blocks from 2000 to 2019, indicates the enhanced status of landscape in the eastern to northern parts of the city. Similar to studies Ajhdari and Taghvaie (2018) analyzed the effect of the spatial configuration of urban cover and physical characteristics of buildings on the cold urban surface islands. They found that lower shape complexity of developed areas and higher building density and fineness of urban areas intensify the urban cold islands, which agrees with the findings of the current study. Also, Sanagar Darbani et al. (2020) investigated the reduction of the effects of urban heat islands on human health through changes in urban form in a hot and dry climate. The findings indicate that as the ratio of height to width increases, the access of sunlight to the environment decreases and as a result the temperature of the environment decreases.

Also, shading caused by the ratio (H/w), the presence of plants and wind in urban valleys can reduce the ambient temperature. In addition, the reduction of impermeable levels of urban coverings and the presence of materials with high albedo causes an increase in evaporation and transpiration, which provides cooling conditions for urban environments and reduces the adverse effects of urban heat on human health.

In line with the research of Pramanik and Punia (2020), who investigated the land use/land cover change and urban heat island intensity based on land surface in Delhi city, India. The results showed that the north, northeast, east and west sub-regions of Delhi are very susceptible to urban heat island severity due to the existence of the industrial zone. In the sub-districts of South and Southwest Delhi, the intensity of the urban heat island was relatively low due to the presence of green spaces. This point was confirmed in the present study.

The results obtained from the landscape analysis in summer 2000, which indicated the improved conditions in the western and southern blocks can be attributed to the composition of the landscape structure with green space and high-rise (shading) buildings. The central fabric of the Birjand city also follows this trend. The dynamic of Birjand after 19 years has improved the landscape of the southern and eastern blocks of the city. The construction of pedestrian streets and dense green space in the health road of Birjand has created favorable weather and reduced the intensity of heat islands. As can be seen in Figure 6(b), the blocks that enjoy favorable landscape quality seem interconnected in the ring road. The dynamic landscape trend of heat islands in the western and northwestern blocks has been due to the conversion of agricultural lands in suburbs to the low-rise buildings and bungalows, which are perceived with qualities reduction or without change. The block in the northwest, which was ranked 14 in

summer 2000, reached the 11th rank with the improved quality in 2019. This evolution is more concerned with the execution of the new national housing project and the conversion of undeveloped lands to residential ones in this region.

The desirable qualities in the western and southern blocks revealed by the landscape analysis in winter 2000 can be due to the greener structures and vegetation. The high-rise buildings have not reduced the intensity of heat islands in winters. Nevertheless, the heat caused by the energy consumption and thermal effect has increased the intensity of heat islands. As can be seen in Equation 6, the blocks with the ranks 1 and 4 in winter 2000 have moved to ranks 6 and 7 with lower quality in winter 2019, due to the construction of high-rise buildings. Furthermore, the completion of the new national housing project and conversion of unimproved lands to semi-tall buildings in the blocks with the ranks 11 and 12 in winter 2000 have improved them to the 7th and 9th ranks in winter 2019. The evolution and dynamism in the east of the city and improved landscape quality have been mostly a function of the conversion of unimproved lands to residential areas with a medium height. The western areas of the city have also experienced a drop in the landscape quality of heat islands with the change of plant-covered lands to residential areas. In a study on landscape metrics using the Landsat satellite images, Gage et al. (2017) concluded that the areas with high vegetation had the lowest LST. Also, Effati et al. (2021) investigated the effects of land use and land cover patterns on land surface temperature using land surface metrics in Tehran, Iran. In this study, the relationship between LULC patterns and land surface temperature was investigated using land surface metrics in Tehran city. For this purpose, Spectral Mixture Analysis (SMA) and Proximity Probability Algorithm were used for LULC map classification. Then the LST zoning map was prepared from the thermal sensor band and classified based on standard deviation and quartile deviation methods. Finally, landform criteria were applied to analyze the relationship between LULC patterns and LST areas. The results showed that LST has a positive correlation with the impervious surface fraction, but it has a negative correlation with the green vegetation fraction. With the increase in the percentage of the surface of the land and the average size of the patches of green space, the temperature decreases, which was confirmed in the present study. In line with the research of Yao et al. (2020), who investigated the impact of urban green space landscape features on seasonal ground surface temperature at the city block scale (urban heat island study in Beijing, China). They used urban blocks as special units for spatial analysis and selected 17 landscape factors, including landscape composition and configuration criteria, as explanatory variables for seasonal land surface temperature. Their results showed that increasing the coverage of urban green space, especially urban forest, is an effective approach to reduce UHI in the urban block. The current study confirms the study by Jafari et al. (2017). They evaluated the relationship between the ecological structure of Neishabour and the pattern of heat islands with an emphasis on the ecological landscape approach. Their findings showed that the four metrics of LPI, LSI, NP, and PLAND had the highest effect and correlation with the LST. Also, in the research of Pan et al. (2019), who investigated the description of the process of urban redevelopment by quantifying the analysis of thermal dynamics and landscape. The aim of this study was to investigate the urban redevelopment efforts by combining UHI remote sensing and land use change. The results showed that the UHI effect had a decreasing trend during the urban development process in the studied area. The results showed that the UHI effect had a decreasing trend during the urban development process in the studied area. Urban heat island intensity can be significantly eliminated or weakened by changes in land use composition and spatial configuration. These phenomena are closely related to redevelopment practices such as industrial displacement and building demolition. This study does not agree with the studies by Tang et al. (2018) on the effect of land use pattern with landscape metrics in the heat island of Changsha, China. Their results revealed that the buildings were the reason behind the rise in

the temperature, while other land uses showed reduced temperatures. This difference may be due to the different climatic characteristics of the two studies.

Recently, many studies have been carried out with the aim of evaluating the relationship between land cover dynamics and heat islands, especially in urban areas, using land cover ecology and remote sensing techniques. These studies stated that the integration of topography metrics and remote sensing provides a reliable assessment that can be useful for urban planning, land use planning and sustainable development goals.

Conclusions

This study aims to evaluate the performance of four thermal island extraction methods and introduce the best method in the study area, as well as recognize and analyze the dynamics of the land scape of thermal islands over time using land scape metrics and remote sensing techniques in the city of Birjand. The results showed that the temperature had a decreasing trend over the past 19 years. The trend of thermal islands in Birjand city from 2000 to 2019 has been decreasing in the north, south and southeast and increasing in the east, west and center of the city. In terms of distribution, the highest temperatures belonged to the unimproved lands and industrial and commercial areas. Moreover, the lowest temperature was in the green spaces and residential areas due to the buildings. The dynamic landscape analysis of heat islands in summers and winters provides the managers and related organizations with proper information to manage and enhance the urban air quality. Given the summer trend and no change or improvement in some blocks (west and northwest), it is suggested to develop the structural composition containing green space accompanied by densely shady high-rise buildings in the city. Furthermore, the installation of high-quality corridors can be known as an urban planning priority, since these paths play the role of desirable air reserves in hot and arid cities. In this regard, the use of continuum landscape models in future studies all around the world is recommended. The results of the winter trend reveal that the green structures and conversion of the unimproved lands to residential semi-tall areas enhance the landscape quality of cities based on heat islands. Meanwhile, with their thermal effect in winter, the high-rise shading buildings reduce the landscape quality in dry climates like Birjand. On the other hand, constructing high-rise buildings and avoiding dispersed construction of villas, along with developing dense green space, have positive effects on the landscape quality of heat islands and city weather in summer. In general, it can be concluded that given the effect of structures on the landscape quality of heat islands, the planning priorities can be consciously used for the wise management of cities.

Acknowledgments We thank the University of Birjand for its spiritual support in conducting this research.

References

Ahmadi, M., Ashorlo, D., and Narangifard, M. (2015). Spatial analysis temperatures the city of Shiraz in the warm seasons and cold using statistical analysis and satellite images. Geographical Researches Quarterly Journal, 30(2), 147-160.

Ahmadi, M., and Dadashi Rudbari, A.A., (2016). Effects of biophysical compounds on the formation of urban thermal islands (Case study of Mashhad). Iranian Journal of Remote Sensing and GIS, 8(3), 39-58.

Alavipanah, S.K. (2007). Thermal remote sensing and its application in earth sciences, second edition, University of Tehran Press.

Aliabadi, K., and Soltanifard, H. (2017). Extracting Vegetation and the Urban Structure of Mashhad Using Newton Interpolation Polynomial and its Relationship with Land Surface Temperature (LST). Iranian Journal of Remote Sensing and GIS, 8(1), 95-108.

Atzberger, C. (2013). Advances in remote sensing of agriculture: Context description, existing operational monitoring systems and major information needs. Remote Sensing, 5(2): 949-981.

Ajhdari, A., and Taghvaie, A. (2018). Analysis of the Effect of Land Cover Spatial Configuration and Physical Characteristics of Buildings on the Surface Urban Cool Island Phenomenon. Journal of Environmental Studies, 44(1), 189-203.

Beigi, S., Mohammadi Sarab, A., Sharifi Kia, M., and Vaghei, M. (2013). Investigation of spatial distribution of thermal islands in Tehran using ETM+ sensor thermal band. The 1st International Conference of IALE Iran.

Chander, G., and Groeneveld, D.P. (2009). Intra-annual NDVI validation of the Landsat 5 TM radiometric calibration. International Journal of Remote Sensing, 30(6), 1621-1628.

Chen, A., Yao, L., Sun, R., and Chen, L. (2014). How many metrics are required to identify the effects of the landscape pattern on land surface temperature?. Ecological Indicators, 45, 424–433.

Chen, Y.C, Chiu, H.W., Su, Y.F., Wu, Y.C. and Cheng, K.S. (2017). Does urbanization increase diurnal land surface temperature variation? Evidence and implications. Landscape and Urban Planning 157, 247-258.

Connors, J. P., Galletti, C. S., and Chow, W. T. L. (2013). Landscape configuration and urban heat island effects: Assessing the relationship between landscape characteristics and land surface temperature in Phoenix, Arizona. Landscape Ecology, 28(2), 271–283.

Estoque, R. C., Murayama, Y., and Myint, S. W. (2017). Effects of landscape composition and pattern on land surface temperature: An urban heat island study in the megacities of Southeast Asia. Science of the Total Environment, 577, 349–359.

Effati, F., Karimi, H., and Yavari, A. (2021). Investigating effects of land use and land cover patterns on land surface temperature using landscape metrics in the city of Tehran, Iran. Arabian Journal of Geosciences, 14(13), 1-13.

Fekrat, H., Asghari Saraskanroud, S., and Alavipanah, S.K. (2020). Estimating the surface temperature of Ardabil land using Landsat images and evaluating the accuracy of the methods of estimating the surface temperature with field data. Remote sensing and geographic information system in natural resources, 11(4), 114-136.

Feng, R., Wang, F., Wang, K., Wang, H., and Li, L. (2021). Urban ecological land and natural-anthropogenic environment interactively drive surface urban heat island: An urban agglomeration-level study in China. Environment International, 157, 106857.

Forman, R.T.T., and Godron, M. (1986). Landscape Ecology, Wiley, New York.

Fouillet, A., Rey, G., Laurent, F., Pavillon, G., Bellec, S., Guihenneuc-Jouyaux, C., Clavel, J., Jougla, and E., Hémon, D. (2006). Excess mortality related to the August 2003 heat wave in France. Internatiol Archives Occupational and Environmental Health 80(1), 16–24.

Gage, E. A., and Cooper, D. J. (2017). Relationships between landscape pattern metrics, vertical structure and surface urban Heat Island formation in a Colorado suburb. Urban Ecosystems, 20(6) 1229–1238.

Harlan, S.L., and Ruddell, D.M., (2011). Climate change and health in cities: impacts of heat and air pollution and potential co-benefits from mitigation and adaptation. Current Opinion in Environmental Sustainability, 3(3), 126–134.

Hennig, C., and Viroli, C. (2015). Quantile-based classifiers, 1–12.

Jafari, E., Soltanifard, H., Aliabadi, K., and Karachi, H. (2017). Investigating the relationships between ecological structure of Neyshabuor city and heat islands patterns with emphasis on landscape ecology approach. Journal of Natural Environment, 70(2), 295-308.

Jafari, S., Alizadeh Shabani, A., Danehkar, Afshin., Nazari Samani, A.A., and Amiri, H. (2015). Theoretical study of concepts, elements and ecological models of Landscape Ecology. Third National Conference of Student Scientific Associations of Agriculture and Resources Natural Karaj.

KarimiFirozjaei, M., Mijani, N., Kiavarz, M., and Alavipanah, S. (2019). An analysis of the thermal effects of built-up and non-built-up lands on each other using reflective and thermal remote sensing data. Journal of Environmental Studies, 45(1), 133-153.

Kupfer, J.A. (2012). Landscape ecology and biogeography rethinking landscape metrics in a post-FRAGSTATS landscape. Progress in Physical Geography: Earth and Environment, 36(3), 400–420.

Lazzarini, M., Marpu, P.R. and Ghedira, H. (2013). Temperature-land cover interactions: The inversion of urban heat island phenomenon in desert city areas. Remote Sensing of Environment, 130, 136-152.

Li, W., Cao, Q., Lang, K., and Wu, J. (2017). Linking potential heat source and sink to urban heat island: Heterogeneous effects of landscape pattern on land surface temperature. Science of the Total Environment, 586, 457-465.

Liu, L., and Zhang, Y. (2011). Urban heat island analysis using the Landsat TM data and ASTER data: A case study in Hong Kong. Remote Sensing, 3(7), 1535–1552.

Mease, D., Wyner, A. J., and Buja, A. (2007). Boosted classification trees and class probability/quantile estimation. Journal of Machine Learning Research, 8, 409–439.

Moghimi, A., Mohammadi, H., Najafian Gorji, M. (2017). Evaluation of temperature change trends, thermal island pattern and vegetation in hot days of Tehran. Natural Geography, 10 (4 (38 consecutive)), 1-18.

Mohammadi, M., and Afifi, M.I. (2021). Investigating the phenomenon of urban heat islands using ASTER satellite images (Study area: Shiraz city). Quarterly Journal of Geography and Environmental Studies, 37(10), 21-44.

Oke, T. R. (1982). The energetic basis of the urban heat island. Quarterly Journal of the Royal Meteorological Society, 108(455), 1-24.

Osaragi, T. (2002). Classification methods for spatial data representation. (CASA Working Papers 40). Centre for Advanced Spatial Analysis (UCL): London, UK.

Pan, Z., Wang, G., Hu, Y., and Cao, B. (2019). Characterizing urban redevelopment process by quantifying thermal dynamic and landscape analysis. Habitat International, 86, 61-70.

Pramanik, S., and Punia, M. (2020). Land use/land cover change and surface urban heat island intensity: source–sink landscape-based study in Delhi, India. Environment, Development and Sustainability, 22(8), 7331-7356.

Qin, Z., Karnieli, A., and Berliner, P. (2001). A mono-window algorithm for retrieving land surface temperature from Landsat TM data and its application to the Israel-Egypt border region. International journal of remote sensing, 22(18), 3719-3746.

Sanagar Darbani, E., Rafiyan, M., Hanaei, T., and Monsefi Prapari, D. (2020). Reducing the effects of urban heat islands on human health through changes in the urban form in the hot and dry climate of Mashhad city (a case study of the checkered texture pattern of Shahid neighborhood and the organic texture of Pachnar neighborhood). Environmental Science and Technology Quarterly, 22(4), 375-387.

Santamouris, M., and Kolokotsa, D. (2016). Urban Climate Mitigation, Routledge, New York.

Shahabifar, M., Assari, M., Kouchakzadeh, M., and Mirlatifi, M. (2010). Iysimetric evaluation of common methods of calculating standard grass reference crop evapotranspiration in greenhouse. Iranian Journal of Water Research in Agriculture, 24(1), 13-19.

Shakiba, A., Ziaian Firoozabadi, P., Ashourloo, D., and Namdari, S. (2009). Analysis of land use and land cover and thermal islands in Tehran, using ETM+ data. Iranian Journal of Remote Sensing and GIS, 1(1), 39-56.

Sobrino, A.J., Jiménez-Muñoz, J.C., and Paolini, L. (2004). Land Surface Temperature Retrieval from LANDSAT TM 5. Remote Sensing of Environment, 90, 434–440.

Sobrino, J.A., Caselles, V., and Becker, F. (1990). Significance of the remotely sensed thermal infrared measurements obtained over a citrus orchard. Journal of Photogrammetric and Remote Sensing, 44(6), 343– 354.

Song, J., Du, S., Feng, X., and Guo, L. (2014). The relationships between landscape compositions and land surface temperature: Quantifying their resolution sensitivity with spatial regression models. In Landscape and Urban Planning, 123, 145–157.

Song, Y., and Wu, C. (2016). Examining the Impact of Urban Biophysical Composition and Neighboring Environment on Surface Urban Heat Island Effect. Advances in Space Research, 57(1), 96–109.

Stone, B., and Rodgers, M.O. (2001). Urban Form and Thermal Efficiency: How the Urban Heat Island Effect. Journal of the American Planning Association, 67(2) 186-198.

Soydan, O. (2020). Effects of landscape composition and patterns on land surface temperature: Urban heat island case study for Nigde, Turkey. Urban Climate, 34, 100688.

Tang, Y., Lan, C., and Feng, H. (2018). Effect analysis of land-use pattern with landscape metrics on an urban heat island. Journal of Applied Remote Sensing, 12(2), 026004.

Turner, B.L. (2010). Sustainability and forest transitions in the Southern Yucatan: the land architecture approach. Land Use Policy, 27, 170–179

Uuemaa, E., Mander, Ü., and Marja, R. (2013). Trends in the use of landscape spatial metrics as landscape indicators: a review. Ecological Indicators, 28, 100-106.

Ulpiani, G. (2021). On the linkage between urban heat island and urban pollution island: Three-decade literature review towards a conceptual framework. Science of the Total Environment, 751, 141727.

Wu, Z., and Ren, Y. (2018). A bibliometric review of past trends and future prospects in urban heat island research from 1990 to 2017. Environmental Reviews, 27, 241–251.

Xiang, Y., Ye, Y., Peng, C., Teng, M., and Zhou, Z. (2022). Seasonal variations for combined effects of landscape metrics on land surface temperature (LST) and aerosol optical depth (AOD). Ecological Indicators, 138, 108810.

Yang, H., and Liu, Y. (2005). A satellite remote sensing based assessment of urban heat island in Lanzhou city, northwest China. International Archives of Photogrammetry. Netherlands: Remote Sensing and Spatial Information Sciences.

Yao, L., Li, T., Xu, M., and Xu, Y. (2020). How the landscape features of urban green space impact seasonal land surface temperatures at a city-block-scale: An urban heat island study in Beijing, China. Urban Forestry and Urban Greening, 52, 126704.

Yu, Z., Yao, Y., Yang, G., Wang, X., and Vejre, H. (2019). Strong contribution of rapid urbanization and urban agglomeration development to regional thermal environment dynamics and evolution. Forest Ecology and Management, 446, 214-225.

Zhou, W., Wang, J., and Cadenasso, M. L. (2017). Effects of the spatial configuration of trees on urban heat mitigation: A comparative study. Remote Sensing of Environment, 195, 1-12.

Zhou, W.Q., Huang, G.L., and Cadenasso, M.L. (2011). Does spatial configuration matter? Understanding the effects of land cover pattern on land surface temperature in urban landscapes. Landscape and Urban Planning, 102, 54–63.

Appendix

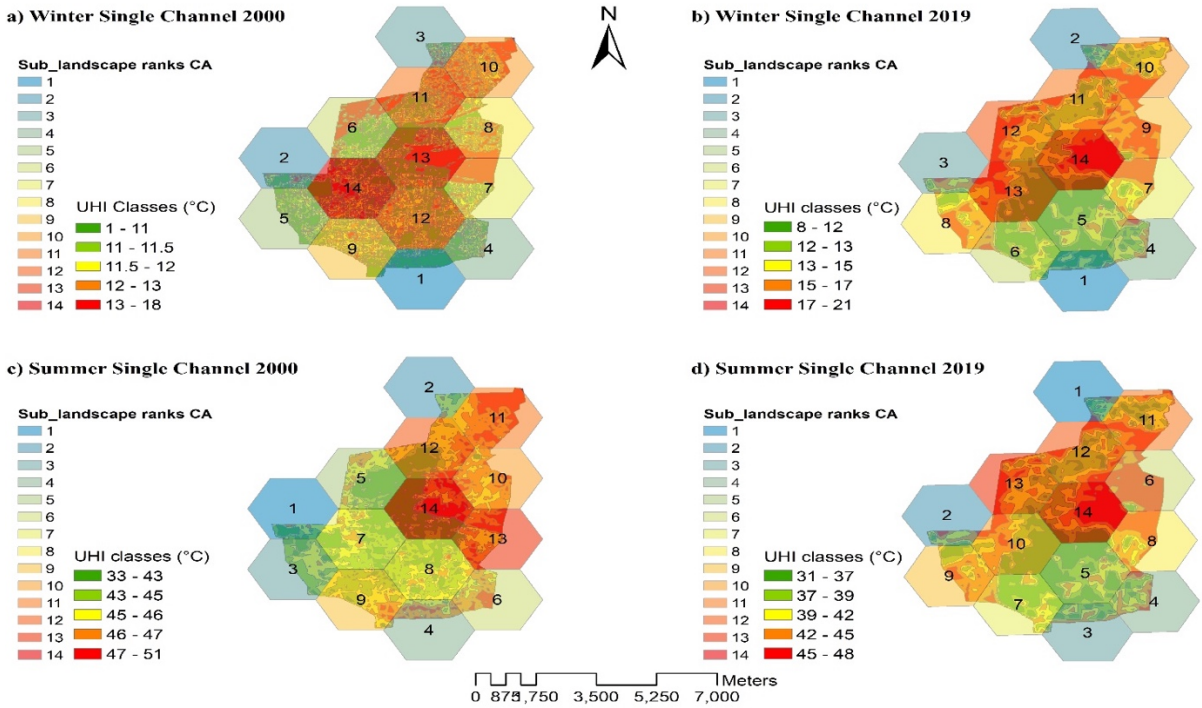

Figure 1s. The summer and winter trend of CA metrics in various periods

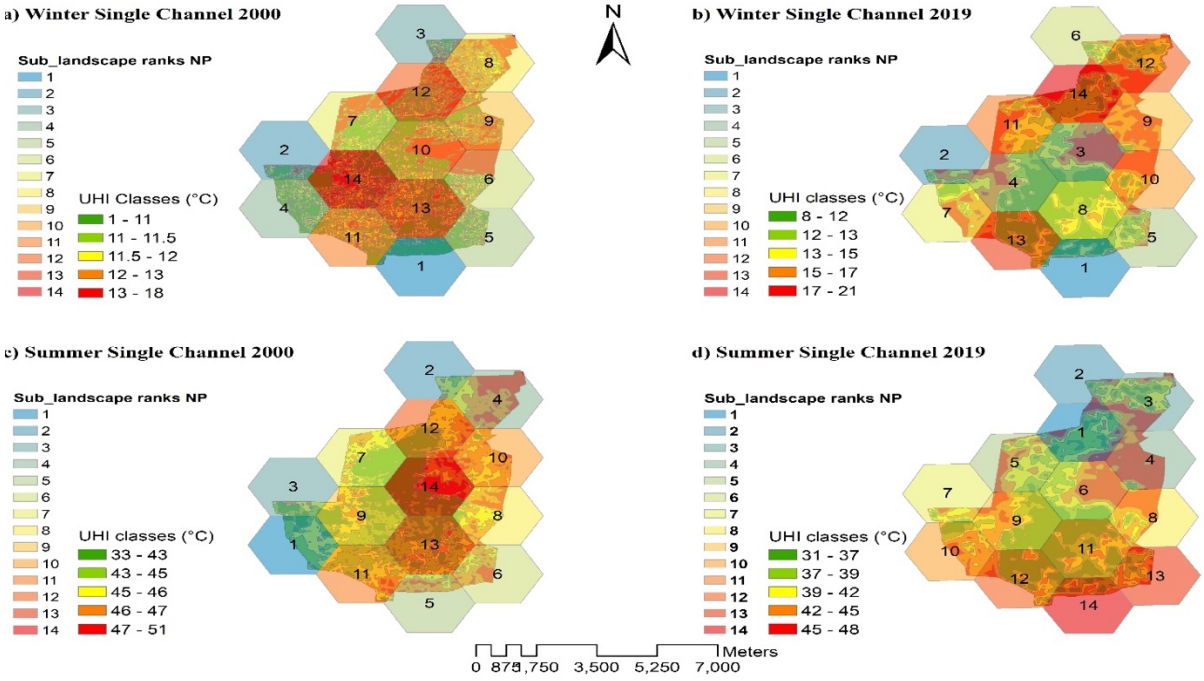

Figure 2s. The summer and winter trends of NP metric in various periods

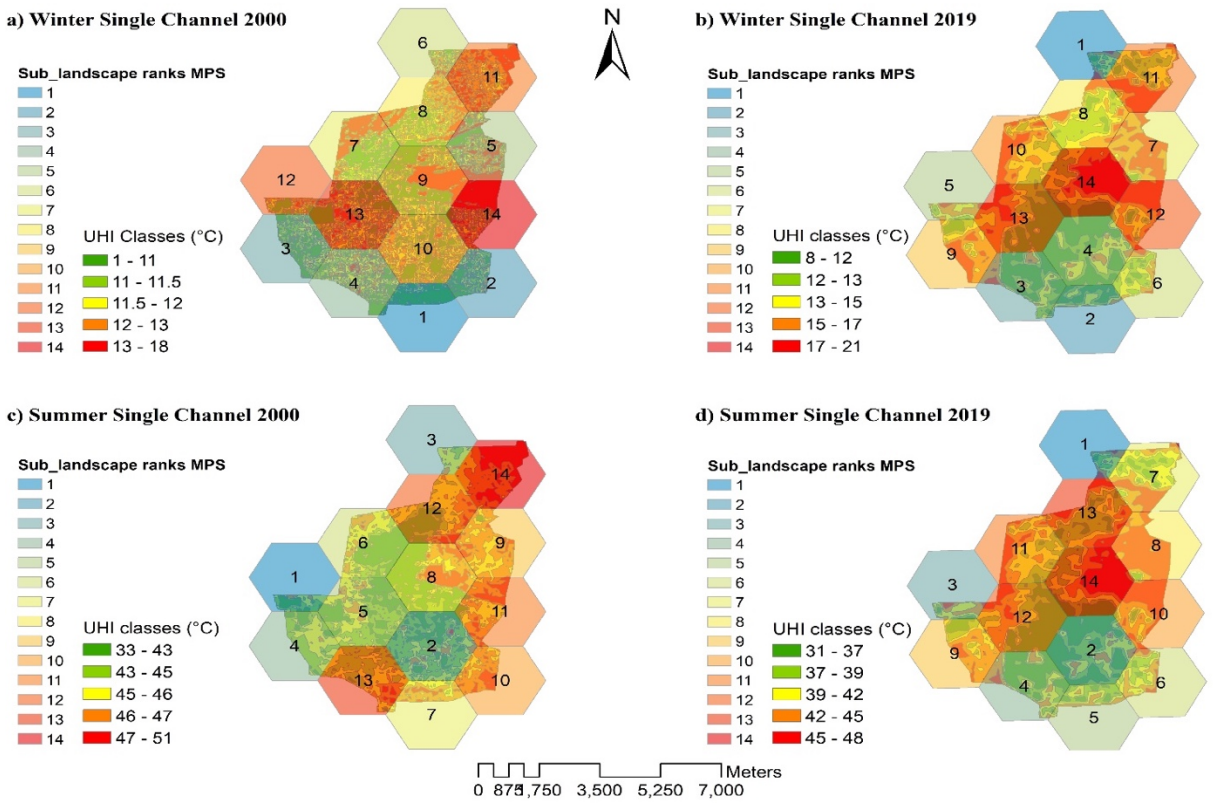

Figure 3s. The summer and winter trends of MPS metric in various periods

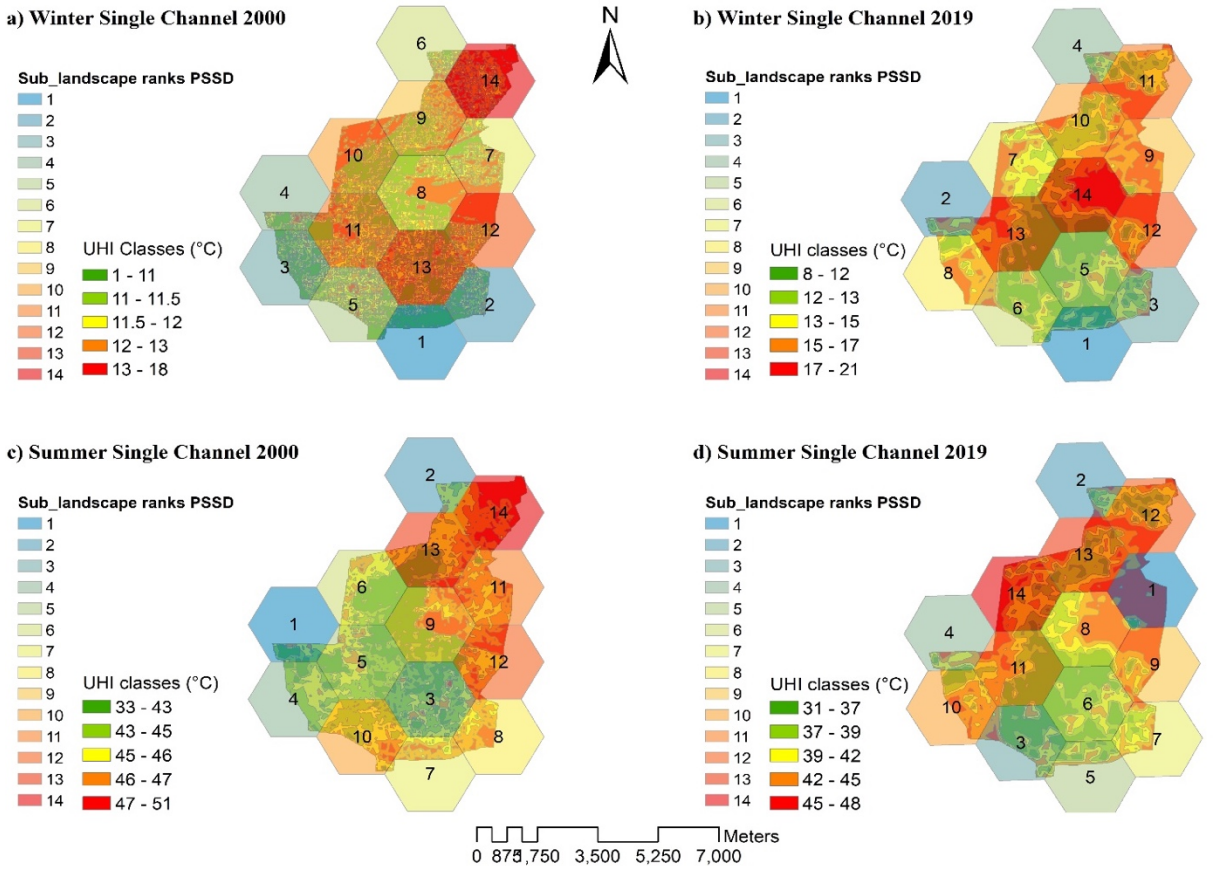

Figure 4s. The summer and winter trends of PSSD metric in various periods

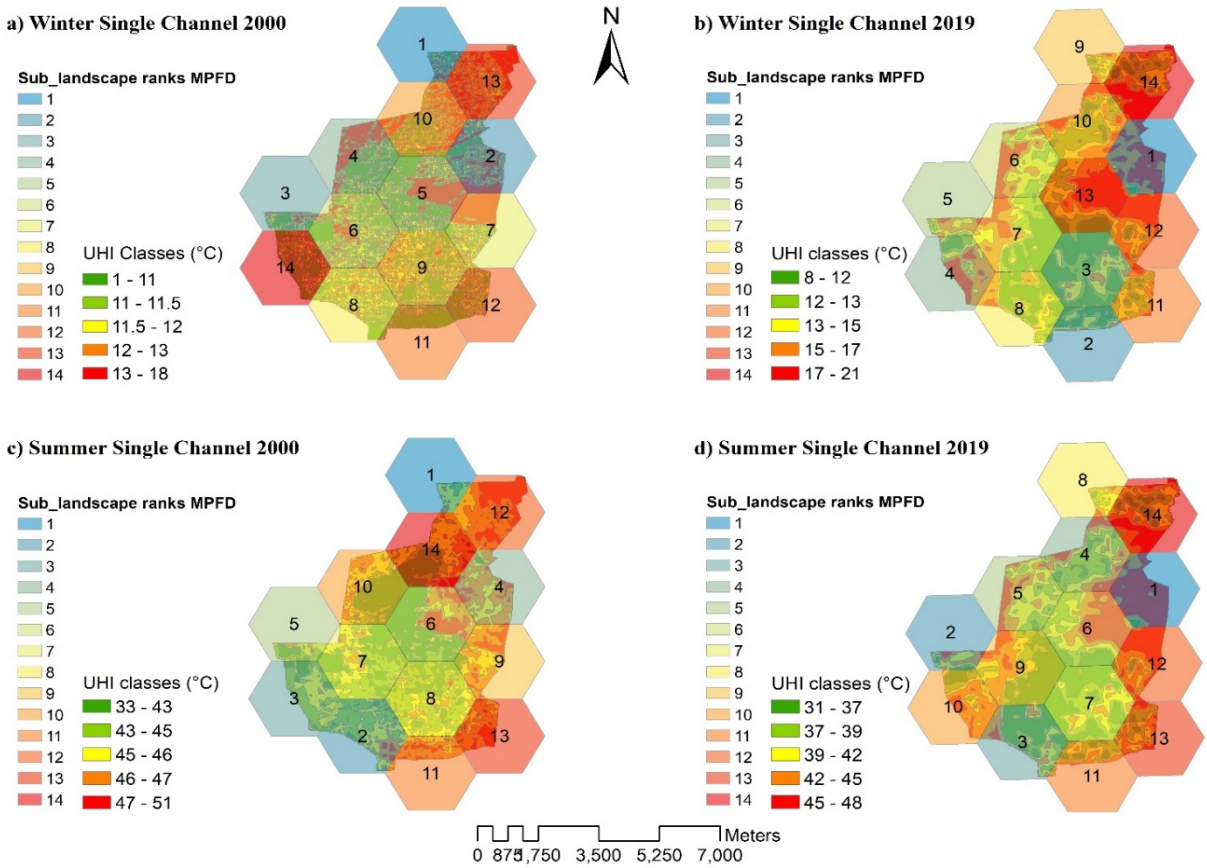

Figure 5s. The summer and winter trends of the MPFD metric in various periods